Meccanica (2016) 51:3015–3023
DOI 10.1007/s11012-016-0518-8

50TH ANNIVERSARY OF MECCANICA

Homotopy between exact coherent structures in shear flows

Masato Nagata

Received: 27 July 2016 / Accepted: 16 August 2016 / Published online: 29 August 2016

Abstract It is found that mirror-symmetric exact coherent structures exist throughout a homotopy continuation path between two canonical flows without linear instability; plane Couette flow and Hagen–Poiseuille flow. Mirror-symmetric exact coherent structures are also identified in plane Poiseuille flow.

Keywords Shear flow instability · Exact coherent structure · Homotopy

Mathematics Subject Classification 76D05 · 76F06 · 76F20 · 76M99

1 Introduction

Study of subcritical transition from laminar to turbulent states in shear flows has attracted significant attention in fluid mechanics in recent years. Among uni-directional shear flows, plane Couette flow (PCF) and Hagen–Poiseuille flow (HPF), are special in that no linear instability of their laminar states exists at any finite Reynolds numbers ([1] for PCF and [2] for HPF), and therefore no smooth transition to other nontrivial equilibrium states is possible according to the *implicit function theorem*. Yet, instabilities are observed in both flows ([3] in PCF and [4] in HPF). This puzzling mathematical property has been presenting fundamental difficulties in understanding how transition to turbulence occurs in these flows from the early 20th century.

In 1990, [5] made a breakthrough by numerically finding nonlinear equilibrium solutions of the Navier–Stokes equations for PCF. The key to the breakthrough was the fact that the linear stability of the laminar flow does not exclude the possibility of nonlinear states that do not have any connection to the laminar flow. This work showed for the first time that nonlinear solutions could abruptly show up via a saddle-node bifurcation at a certain finite Reynolds number. More specifically, in [5], the solution branch is continued from a rotating flow problem where the linear instability of the laminar state exists and thus nonlinear solution branches can be followed successively by bifurcation analysis. Then, one of the nonlinear solution branches has been successfully continued to the original no-rotation problem. This strategy to find a nonlinear solution of one system through a continuous deformation of the known solution of another system, is called *homotopy* method. About a decade later,

M. Nagata (✉)
Department of Aeronautics and Astronautics, Graduate School of Engineering, Kyoto University, Katsura, Nishikyo-ku, Kyoto 615-8540, Japan
e-mail: nagata@kuaero.kyoto-u.ac.jp

M. Nagata
Department of Mechanics, School of Mechanical Engineering, Tianjin University, Nankai District, Tianjin 300072, People's Republic of China

nonlinear solutions on such disconnected branches were found in HPF as well [6, 7].

As various nonlinear states in various shear flows became available (e.g. [8–10] in PCF, [11–13] in plane Poiseuille flow (PPF), and [14] in HPF), the study of such nonlinear solutions, called *exact coherent structures* (ECS), has gathered considerable attention because it may offer a new way to explain subcritical transition to turbulence in shear flows. Our particular attention in the current article is focused on seeking possible nonlinear solution links between the available ECS's in PCF , PPF and HPF.

2 Formulation of the problem

We consider the motion of an incompressible viscous fluid with the constant density ρ and kinematic viscosity ν between two horizontal parallel plates of infinite extent separated by the distance $2d^*$, subject to a system rotation of constant rate Ω^* about a spanwise axis. The motion is induced by moving the plates in the opposite directions with a constant speed U^* (PCF) and/or applying a constant pressure gradient G^* in the direction of the motion of the bottom plate (PPF). Adopting a Cartesian coordinate with origin on the mid-plane between the plates, we non-dimensionalise the Navier–Stokes equations and incompressibility condition expressed in the rotating frame of reference:

$$\frac{\partial u}{\partial t} + (u\cdot\nabla)u = -\nabla p + \nabla^2 u - \Omega\times u, \tag{1}$$

$$\nabla\cdot u = 0. \tag{2}$$

In these expression velocity u has components u_i in the x_i direction, $u=[u_1,u_2,u_3]=[u,v,w]$, where $x_1=x, x_2=y$ and $x_3=z$ denote the streamwise, spanwise and wall-normal directions, respectively, t denotes time and p is a modified pressure that includes the centrifugal force term. All lengths and time have been scaled by the half-gap d^* and the viscous diffusion time d^{*2}/ν, respectively, while velocities has been scaled by ν/d^*. The rotation number $\Omega := 2\Omega^* d^{*2}/\nu$ has been introduced, where $\Omega=[0,\Omega,0]$ denotes the system rotation vector.

Subject to no-slip boundary condition at the plates a laminar basic flow solution is given by $u=U_B=[U_B(z),0,0]$, in which $U_B=-Re\,z+R_P(1-z^2)$ where $Re := U^* d^*/\nu$ is the Reynolds number induced by the motion of the plates, and $R_P := G^* d^{*3}/2\rho\nu^2$ is the Reynolds number induced by the pressure gradient.

The total flow field is decomposed into the basic state and a disturbance flow field $\{\tilde{u},\tilde{p}\}$, which satisfies

$$\frac{\partial\tilde{u}}{\partial t} + (U_B\cdot\nabla)\tilde{u} + (\tilde{u}\cdot\nabla)U_B + (\tilde{u}\cdot\nabla)\tilde{u} = -\nabla\tilde{p} + \nabla^2\tilde{u} - \Omega\times\tilde{u}, \tag{3}$$

$$\nabla\cdot\tilde{u} = 0, \tag{4}$$

subject to the boundary condition, $\tilde{u}=\mathbf{0}$ at $z=\pm1$.

Following [15] we express $\tilde{u}$ as

$$\tilde{u} = \overline{\tilde{u}}\hat{i} + \nabla\times\nabla\times(\phi\hat{k}) + \nabla\times(\psi\hat{k}), \tag{5}$$

where $\overline{\cdot} \equiv \frac{\alpha\beta}{4\pi^2}\int_0^{\frac{2\pi}{\alpha}}\int_0^{\frac{2\pi}{\beta}}\cdot\,\mathrm{d}x\,\mathrm{d}y$ denotes the average over the periodic domain given by the streamwise and spanwise wavenumbers, α and β. Note that the expression (5) ensures the incompressible condition (4). The equations for the scalar variables, ϕ,ψ and $\overline{\tilde{u}}$, are obtained by operations, $\hat{k}\cdot\nabla\times\nabla\times(3)$, $\hat{k}\cdot\nabla\times(3)$ and $\hat{i}\cdot\overline{(3)}$, respectively. The boundary condition (4) becomes $\overline{\tilde{u}}=\phi=\partial_z\phi=\psi=0$ at $z=\pm1$.

In order to solve the resulting three partial differential equations numerically we expand the scalar variables ϕ,ψ and $\overline{\tilde{u}}$ by the following truncated sums:

$$\phi(x,y,z;t) = \sum_{\substack{m=-M\\(m,n)\neq(0,0)}}^{M}\ \sum_{n=-N}^{N} \sum_{\ell=0}^{L} X^{(1)}_{\ell mn}\Phi_\ell(z)\exp[\mathrm{i}(\mathrm{m}\alpha(\mathrm{x}-\mathrm{ct})+\mathrm{n}\beta\mathrm{y})], \tag{6}$$

$$\psi(x,y,z;t) = \sum_{\substack{m=-M\\(m,n)\neq(0,0)}}^{M}\ \sum_{n=-N}^{N} \sum_{\ell=0}^{L} X^{(2)}_{\ell mn}\Psi_\ell(z)\exp[\mathrm{i}(\mathrm{m}\alpha(\mathrm{x}-\mathrm{ct})+\mathrm{n}\beta\mathrm{y})], \tag{7}$$

$$\overline{\tilde{u}}(z) = \sum_{\ell=0}^{L} X^{(3)}_{\ell 00}U_\ell(z), \tag{8}$$

where the basis functions, $\Phi_\ell = (1-z^2)^2 T_\ell(z)$ and $\Psi_\ell = U_\ell = (1-z^2)T_\ell(z)$ with $T_\ell(x)$ being the ℓ-th Chebyshev polynomial of the first kind, satisfy no-slip condition at $z = \pm 1$. Here, we have assumed that $\tilde{u} = (\tilde{u}, \tilde{v}, \tilde{w})$ and $\tilde{p}$ take a travelling-wave form propagating in the streamwise direction with the wave speed c,

After substituting (6), (7) and (8) into the three partial differential equations, we discretize the equations by using a standard Chebyshev-collocation and Fourier–Galerkin technique, namely the equations projected on the x- and y-directions, are evaluated at the collocation points, $z_\ell = \cos\left(\frac{\ell+1}{L+2}\pi\right), (\ell = 0, \ldots, L)$. Then, we solve the resulting quadratic algebraic equations for the spectral coefficients $X^{(j)}_{\ell mn}, (j = 1, 2, 3)$ by the Newton–Raphson iteration method. The wave speed c is unknown, but it can be swapped with the real or imaginary part of an appropriate $X^{(j)}_{\ell mn}$ by resetting the origin of time t.

The momentum transport on the top plate,

$$M := -\left.\frac{U_B' + \overline{\tilde{u}}'}{U_B'}\right|_{z=1}, \tag{9}$$

where the prime denotes the differentiation with respect to z, and the friction factor,

$$\lambda := \frac{2d^* G^*}{\rho U_m^{*\,2}}, \tag{10}$$

are chosen as nonlinear measures (see [16] for further computational details).

3 Exact coherent structures in plane Couette flow and plane Poiseuille flow

In this section we first establish nonlinear solution branches in the rotating problems. Then, by treating the rotation number Ω as a homotopy parameter, solutions on the solution branches are followed as $\Omega \to 0$ so as to recover ECS's in PCF and PPF.

3.1 Rotating plane Couette flow

No linear instabilities are known to PCF. However, the flow can be linearly unstable subject to a system rotation about a spanwise axis. The linear stability of rotating plane Couette flow to a streamwise-independent perturbation is determined by a single parameter, called the Taylor number $Ta := \Omega(Re - \Omega)$.

Figure 1a shows two loci of the critical Taylor numbers, $Ta = Ta_c^{(1)} = 106.735$ and $Ta = Ta_c^{(2)} = 1100.650$, on the (Ω, Re)-plane, at which nonlinear streamwise-independent flows bifurcate. The corresponding critical spanwise wavenumbers are $\beta_c^{(1)} = 1.5582$ and $\beta_c^{(2)} = 2.6823$, respectively. Typical nonlinear states, referred to as Taylor vortex flow type I (TV_1) and type II (TV_2), are presented in Fig. 1b. It is found that TV_1 is characterised by a single-layered array of vortex rolls, in comparison with a double-layered array for TV_2. Three-dimensional tertiary flows bifurcate from these secondary flows. With a suitable choice of parameters, Re, Ω, α and β, tertiary solution branches reach the line of $\Omega = 0$, creating nonlinear solutions of PCF, as exemplified in Fig. 2.

The tertiary solution branch, denoted by WVF in Fig. 2, corresponds to the wavy vortex flow in the Taylor–Couette system. The solution at $\Omega = 0$ on WVF, called Nagata solution [5], is discovered for the first time as described in Introduction. The solution on the other tertiary solution branch, denoted by Ribbon in the figure, is characterised by the spanwise mirror-symmetry [17]. Although the existence of Ribbon had been recognized by [18], the mirror-symmetric solutions of PCF themselves were found recently by means of different types of homotopy approaches [8, 9].

When $\Omega = 0$, these two types of solutions appear via a saddle-node bifurcation as shown in Fig. 3. Nagata solution in Fig. 3a is known to possess the following symmetries, the *shift-reflection symmetry*,

$$S : [u, v, w](x, y, z) = [u, -v, w](x + \pi/\alpha, -y + \pi/\beta, z), \tag{11}$$

and the *shift-rotation symmetry*,

$$\Omega : [u, v, w](x, y, z) = [-u, v, -w](-x, y + \pi/\beta, -z). \tag{12}$$

The mirror-symmetric solutions in blue in Fig. 3b possess an additional symmetry, called the *mirror-symmetry*,

$$Z_y : [u, v, w](x, y, z) = [u, -v, w](x, -y, z). \tag{13}$$

We denote these solutions by $\mathscr{P}^*_{pcf}$ and $\mathscr{M}^*_{pcf}$ (an asterisk indicating the steady state), respectively. Also

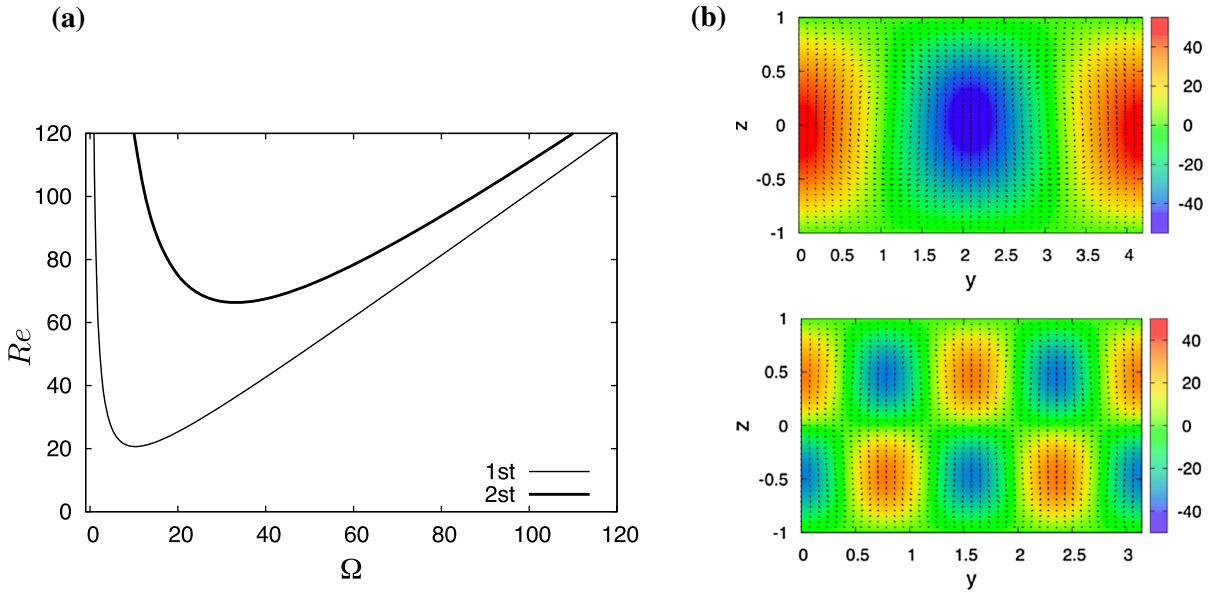

Fig. 1 **a** The loci of the critical Taylor numbers, $Ta = Ta_c{}^{(1)} = 106.735$ (*thin curve*) and $Ta = Ta_c{}^{(2)} = 1100.650$ (*thick curve*). **b** The cross-sectional flow of streamwise-independent flows, TV_1 (*top*) at $Ta = 150$ with $\beta = 1.56$ and TV_2 (*bottom*) at $Ta = 1200$ with $\beta = 2.68$ in the (y, z)-plane. $-\pi/\beta \le y \le \pi/\beta$ and $-1 \le z \le 1$. *Arrows* and *contours* represent the cross-sectional velocities, $(\tilde{v}, \tilde{w})$ and the streamwise velocity, $\tilde{u}$, respectively

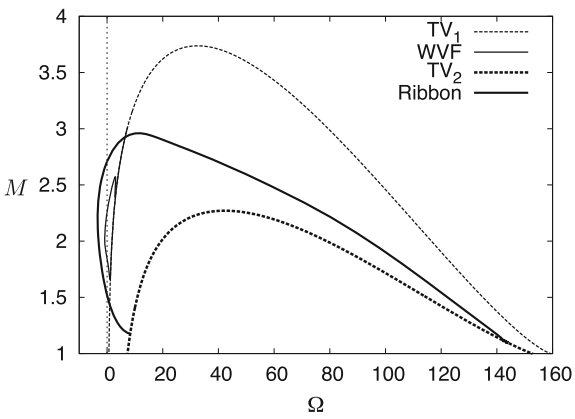

Fig. 2 The bifurcation diagram of rotating plane Couette flow at $Re = 160$. $\beta = 1.5$ for TV_1, $\beta = 3.0$ for TV_2 and $(\alpha, \beta) = (0.9, 1.5)$ for WVF and Ribbon

shown in red in Fig. 3b is the travelling-wave solution branch, which is found during the continuation approach from plane Couette flow to sliding Couette flow to be discussed in Sect. 5.1 below. This solution is denoted by $\mathcal{M}_{pcf}$ since the mirror-symmetry is preserved.

3.2 Rotating plane Poiseuille flow

In contrast to PCF, PPF can be linearly unstable. The critical Reynolds number R_{Pc} is 5772.22 for a spanwise-independent perturbation and the corresponding critical streamwise wavenumber is $\alpha_c = 1.02$.

With the inclusion of a spanwise system rotation Ω, the critical Reynolds number is reduced drastically. Streamwise-independent perturbations cause this instability. [19] calculated $(R_{Pc}, \beta_c) = (66.40, 2.45)$ when $\Omega = 22.133$. Figure 4 shows that the marginal stability curve corresponding to $(\alpha, \beta) = (0, 2.5)$ attains the smallest Reynolds number among other combinations of wavenumbers in the figure. Secondary flows bifurcate from these marginal curves. Figure 5a shows the bifurcations of three-dimensional tertiary flows, $\mathcal{G}_1, \ldots, \mathcal{G}_5$, from the two-dimensional secondary flow $\mathcal{D}_1$ with $\beta = 2.5$ when $\Omega = 22.1325$. Three-dimensional flows can also bifurcate direct from the basic laminar state as exemplified by $\mathcal{G}_{11}, \ldots, \mathcal{G}_{15}$ in Fig. 5b.

Among fifteen nonlinear solution branches $\mathcal{G}_1, \ldots, \mathcal{G}_{15}$, detected by [16], only $\mathcal{G}_1$ and $\mathcal{G}_{13}$ were

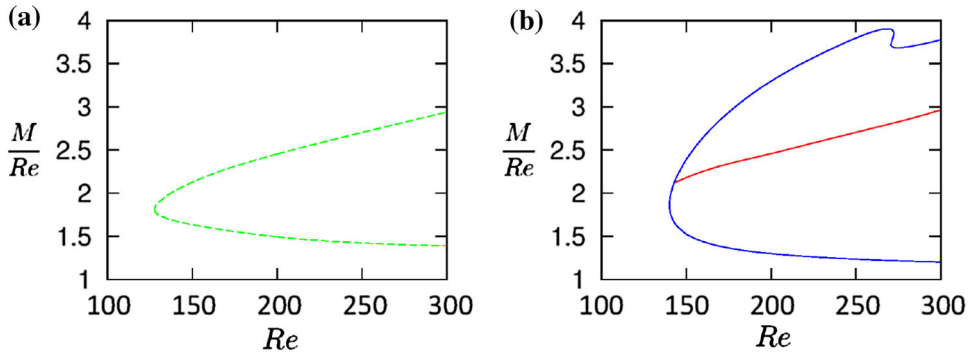

Fig. 3 The saddle-node bifurcation of plane Couette flow solutions at the optimal wavenumber pair. **a** $\mathscr{P}^*_{pcf}$; $R_{opt} = 127.7, (\alpha_{opt}, \beta_{opt}) = (0.58, 1.15)$. **b** $\mathscr{M}^*_{pcf}$ in *blue* and $\mathscr{M}_{pcf}$ in *red*; $R_{opt} = 137, (\alpha_{opt}, \beta_{opt}) = (0.75, 1.37)$

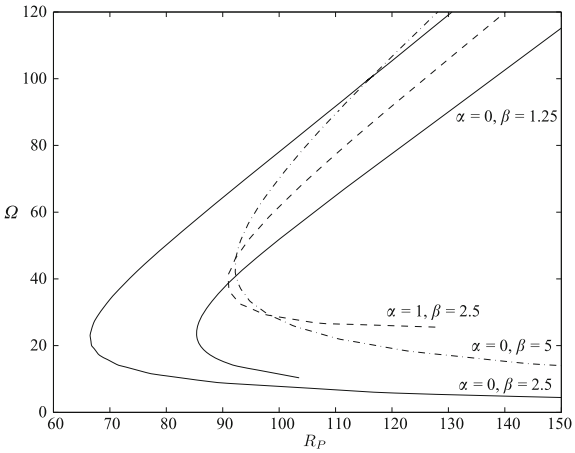

Fig. 4 Marginal stability curves in rotating plane Poiseuille flow for perturbations with (α, β) indicated

found to reach $\Omega = 0$. These two states are called TW1 and TW2. Furthermore, [16] found a third state, called TW3, which bifurcated from TW1.

The shift-rotation symmetry (12) is broken for all of these three solutions because of the symmetric flow profile, $U_B(-z) = U_B(z)$, for PPF. TW1 possesses the shift-reflection symmetry S only, while TW2 possesses the symmetry S and the mirror symmetry Z_y. TW3 possesses the symmetry S and a new symmetry Z_{yz},

$$Z_{yz} : [u, v, w](x, y, z) = [u, -v, -w](x, -y + \pi/\beta, -z). \tag{14}$$

The saddle-node bifurcations of these nonlinear states are shown in Fig. 6.

4 Homotopy from plane Couette flow to plane Poiseuille flow

Homotopy continuation from PCF to PPF is straightforward by adjusting two Reynolds numbers, Re and R_P. As soon as the Poiseuille component is added the shift-rotation symmetry (12) is broken.

Nagata solution, $\mathscr{P}^*_{pcf}$, in PCF was used as a starting solution for the homotopy by [11], who considered the combination of the two Reynolds numbers as

$$U_B(z) = -R_0\, z - \mu R_0(1/6 - z^2/2), \tag{15}$$

where PCF is given when the homotopy parameter $\mu = 0$ with $R_0 = Re$. The half channel PPF is retrieved in $z \in [-1, 1]$ with $\frac{dU_B}{dz}|_{z=1} = 0$ when $\mu = 1$ with $R_0 = R_P$. The flow which reached the PPF limit is referred to as W03 here. W03 inherits the shift-reflection symmetry of Nagata solution. With the half channel restriction, W03 is bound to possess the top-bottom symmetry, Z_z, additionally:

$$Z_z : [u, v, w](x, y, z) = [u, v, -w](x, y, -z). \tag{16}$$

The steady and travelling-wave mirror-symmetric states, $\mathscr{M}^*_{pcf}$ and $\mathscr{M}_{pcf}$, in PCF were continued to PPF by [12], where the basic flow,

$$U_B(z) = -\sqrt{1-\mu}Re\, z + \sqrt{\mu}R_P(1 - z^2), \tag{17}$$

is considered. The solution that reached the PPF limit was referred to as MS-S in [12] and had symmetries, S, Z_y and Z_z. [12] also found another mirror-symmetric state, called MS-A, which bifurcated from MS-S. The top-bottom symmetry Z_z was broken for MS-A. The

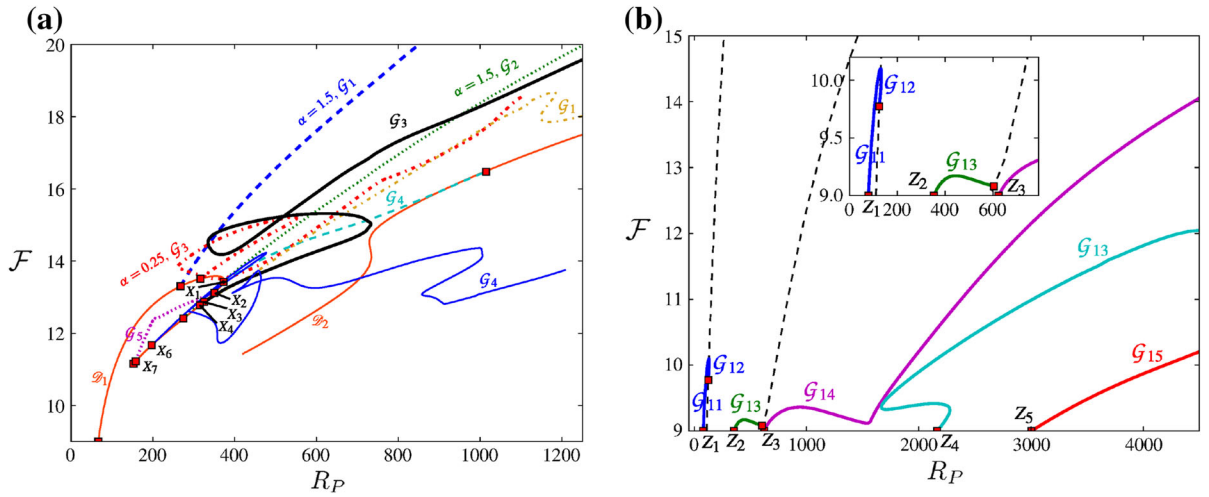

Fig. 5 Bifurcation of three-dimensional flows in rotating plane Poiseuille flow at $\Omega = 22.1325$. The nonlinear measure is friction factor $\mathcal{F} = R_P\lambda$. **a** Tertiary flows, $\mathcal{G}_1, \ldots, \mathcal{G}_5$, bifurcating from the two-dimensional secondary flow $\mathcal{D}_1$ with $\beta = 2.5$. **b** Three-dimensional secondary flows, $\mathcal{G}_{11}, \ldots, \mathcal{G}_{15}$, bifurcating direct from the basic state

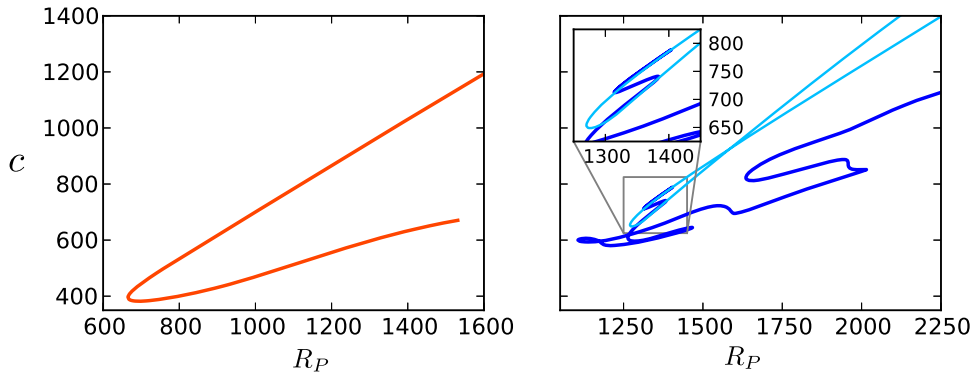

Fig. 6 The saddle-node bifurcations of (*left*): TW2 (*in red*) and (*right*): TW1 (*in dark blue*) and TW3 (*in light blue*) for the optimal wavenumber pair. TW1: $(\alpha_{opt}, \beta_{opt}) = (1.63, 3.25)$. TW2: $(\alpha_{opt}, \beta_{opt}) = (1.32, 2.89)$. The nonlinear measure is the wave speed c

saddle-node bifurcations of these solutions are presented in Fig. 7.

5 Homotopy continuation from plane Couette flow to Hagen–Poiseuille flow

A nonlinear solution link between PCF and HPF is sought in this section. We choose sliding Couette flow (SCF), i.e. flow between concentric cylinders in mutual relative motions in the axial directions, as an intermediate between these two flows that are very different geometrically.

5.1 Homotopy from plane Couette flow to sliding Couette flow

As in the previous section we consider an incompressible viscous motion of fluid with the density ρ and kinematic viscosity ν. Fluid occupies the gap between two infinitely long concentric cylinders with radii a^* and $b^*(=a^* + 2d^*)$. The flow is driven by moving the cylinders in the opposite axial directions with the same speed U^* and/or applying an axial pressure gradient G^*. Subject to no-slip on the cylinders, the basic flow in non-dimensional form is given by

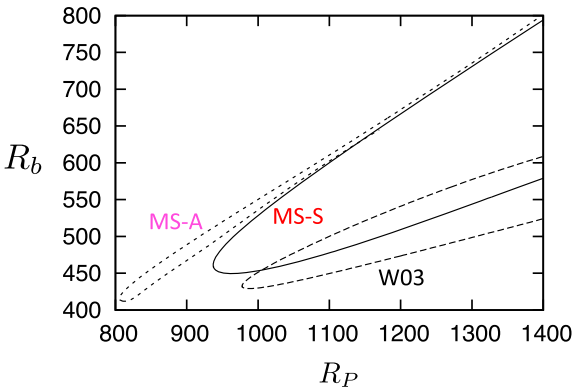

Fig. 7 The saddle-node bifurcations of MS-S, MS-A and W03 for the optimal wavenumber pair. MS-S: $(\alpha_{opt}, \beta_{opt}) = (1.47, 3.06)$. MS-A: $(\alpha_{opt}, \beta_{opt}) = (1.33, 1.73)$. W03: $(\alpha_{opt}, \beta_{opt}) = (1.02, 2.64)$. The nonlinear measure is the bulk Reynolds number $R_b := \frac{\alpha\beta}{8\pi^2}\int_0^{2\pi/\alpha}\int_0^{2\pi/\beta}\int_{-1}^{+1}(U_B + \bar{\tilde{u}})\ \mathrm{d}x\,\mathrm{d}y\,\mathrm{d}z$

$$U_B(r) = -Re\frac{2\ln(r/r_0) - \ln\eta}{\ln\eta} + R_P\frac{r^2 - r_o^2 - 2r_p^2\ln(r/r_o)}{2}, \tag{18}$$

where $\eta = r_i/r_0$ is the radius ratio with r_i and r_0 being the inner and outer cylinder radii, respectively. Re is the Reynolds number induced by the sliding motion of the cylinders and R_P is the Reynolds number induced by the axial pressure gradient, defined by $Re := U^* d/\nu$ and $R_P := G^* d^3/2\rho\nu^2$, respectively, as in the planer case. U_B takes its maximum value at $r = r_p = r_o\sqrt{(\eta^2-1)/(2\ln\eta)}$ when $Re = 0$.

As in the last section we superimpose disturbances on the basic flow. Disturbances are decomposed into a mean part and residuals with toroidal and poloidal potentials. They are expressed by a Fourier–Chebyshev spectral expansion. To discretize the disturbance equations, collocation method is used. The resultant algebraic equations for the expansion coefficients are solved numerically by Newton's method. The momentum transport $M := -(r_0/r_m)(U_B + \bar{\tilde{u}})'|_{r=r_0}$ on the outer cylinder is chosen as a nonlinear measure of the solution where $r_m = (1+\eta)/(1-\eta)$ is the mean radius.

A continuation to SCF has been made by using the steady mirror-symmetric solution $\mathscr{M}^*_{pcf}$ in PCF. The upper and the lower branch $\mathscr{M}^*_{pcf}$ solutions, indicated by black dots in Fig. 8 are the starting points. The orange arrows in the figure indicate the continuation directions taken, where the radius ratio η is a homotopy parameter. In the annulus geometry, $\mathscr{M}^*_{pcf}$ solution in the plane geometry turns into a travelling-wave form. It possesses the shift-reflection symmetry,

$$S : [u, v, w](x, \theta, r) = [u, -v, w](x + \pi/\alpha, -\theta + \pi, r), \tag{19}$$

and the mirror-symmetry,

$$Z_\theta : [u, v, w](x, \theta, r) = [u, -v, w](x, -\theta, r). \tag{20}$$

The shift-rotation symmetry is broken because the reflection about the mean radius $r = r_m$ corresponding to $z = 0$ in (12) becomes asymmetric due to the curvature in the cylindrical coordinates. We denote this travelling-wave solution by $\mathscr{M}_{scf}$.

As can be seen in Fig. 8, this particular attempt was not successful in the sense that the continuation routes did not reach the wide gap limit, $\eta \to 0$. Instead, the routes turned back and ended up at the blue dot in the PCF limit, producing the travelling-wave form of the mirror-symmetric solution $\mathscr{M}_{pcf}$ as a by-product [10].

The homotopy continuation using Nagata solution $\mathscr{P}^*_{pcf}$ was attempted by [20]. It is shown there that the continued solution branch $\mathscr{P}_{scf}$ terminates on a mirror-symmetric travelling-wave solution branch $\mathscr{M}_{scf}$. This mirror-symmetric branch separates into two solution branches with different flow structures in a complicated manner in the wavenumber space: one of them preserves the same single-layered vortical structure as Nagata solution and the other exhibits a double-layered vortical structure. It turns out that the latter

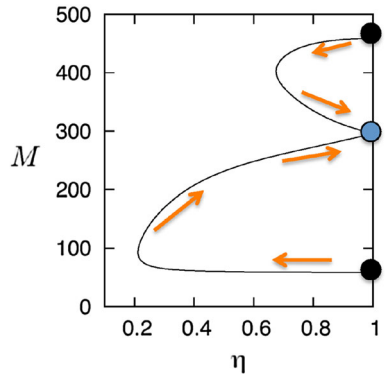

Fig. 8 Homotopy from the steady mirror-symmetric solution $\mathscr{M}^*_{pcf}$ (*black dots*) in PCF to SCF. $Re = 200, (\alpha, \beta) = (0.75, 1.37)$

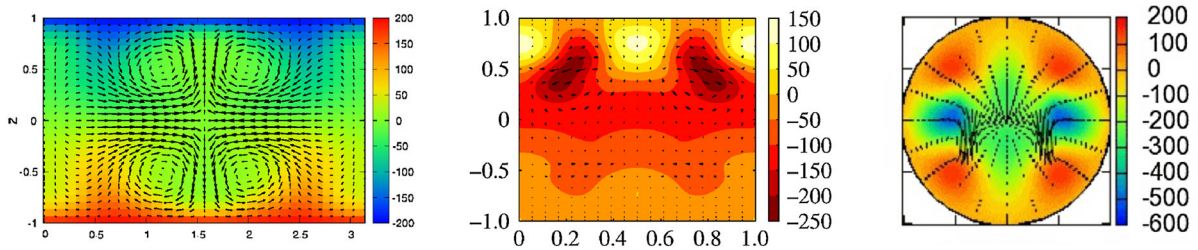

Fig. 9 Snap-shots of the lower branch mirror-symmetric flow fields. From *left* to *right*, $\mathscr{M}^*_{pcf}$ in PCF: ($Re = 200, \alpha = 1.0, \beta = 2.0$), TW2 in PPF: ($R_P = 1200, \alpha = 1.32, \beta = 2.89$) and HPF ($R_b = 600, \alpha = 0.72$. The polar coordinate (r, θ) is rotated by 90° anti-clockwise.). Colour indicates the streamwise velocity

belongs to the branch that approached $\eta \approx 0.2$ in Fig. 8.

5.2 Homotopy from sliding Couette flow to Hagen–Poiseuille flow

The following two steps are required for the homotopy from SCF to HPF:

(I) To add an axial pressure gradient so that the basic velocity profile becomes a parabola-like shape.
(II) To eliminate the inner cylinder.

For the requirement (I), we gradually increase the pressure-based Reynolds number, R_P, until the constraint

$$\frac{R_P}{Re} = \frac{2}{(r_i^2 - r_p^2)\ln \eta} \tag{21}$$

is met for a fixed Re. With this constraint the basic flow profile (18) becomes a parabola-like shape with vanishing shear on the inner cylinder, *i.e.* $\mathrm{d}\, U_B(r)/\,\mathrm{d}\, r|_{r=r_i} = 0$. This choice of the basic flow is convenient because the profile coincides with that of HPF, $U_B(r) = R_P(r_o^2 - r^2)/2 + Re$, in the limit $\eta \to 0$. Recall that the pipe is moving in the axial direction with a constant speed Re.

Regarding the requirement (II), we remove the no-slip boundary effect on the disturbances and ensure the regularity of the flow at the pipe centre. In order for a function, expressed by a truncated series of the ℓ-th polynomial basis functions as

$$f(r,\theta) = \sum_{\ell=0}^{\infty} \sum_{m=-\infty}^{\infty} a_{lm} P_\ell^m(r)\ \mathrm{e}^{\ im\theta}, \tag{22}$$

to be regular at $r = 0$, the following two conditions must be satisfied by $P_\ell^m(r)$ [21].

(a) Parity condition: If m is an odd/even integer, $P_\ell^m(r)$ must be an odd/even function.
(b) Order condition: The minimum order of $P_\ell^m(r) \geq |m|$.

For the disturbance flow field (5), it can be shown that $\phi/r, \psi/r$ and $\tilde{\bar{u}}$ must satisfy the regularity conditions. This leads to new basis functions Φ_ℓ, Ψ_ℓ and U_ℓ. Accordingly, we introduce another homotopy parameter ϵ which bridges the two sets of basis functions, one for no-slip and the other for regularity at $r = 0$ (see [22] for detail).

Now, we complete our homotopy continuation to HPF by increasing ϵ from zero to 1 for the mirror-symmetric solution $\mathscr{M}_{scf}$ obtained in the annular geometry with vanishingly thin inner cylinder, $\eta = 0$ [23]. We find that $\alpha = 0.73$ for $m = 1$ optimises the bulk Reynolds number, $R_b = \int_{r_i}^{r_o}(U_B + \bar{\tilde{u}})rdr/2 = 192.85$. These values agree well with those of the M1 solution (mirror-symmetric solution with m =1) in HPF found by [14]: $R_{PK} = 773 (= 4 \times 193.25)$ at $\alpha_{PK} = 1.44 (= 2 \times 0.72)$. Note that their length scale is different from ours: $R_{PK} = 4R_b$ and $\alpha_{PK} = 2\alpha$. We claim that our mirror-symmetric solution corresponds to M1.

6 Concluding remarks

A homotopy of exact coherent structures between PCF, PPF and HPF is established by developing continuous deformations between planar and circular cross-sectional shear flows. It is found that mirror-

symmetric solutions exist continuously throughout the homotopy route (see Fig. 9).

The TW2 solution provides, to our knowledge, the lowest Reynolds number at which PPF solutions other than the basic flow are known to exist (the solution appears in a saddle-node bifurcation at $R_P = 665$). It is confirmed by [13] that the upper TW2 solution branch terminates on the MS-S branch of [12]. However, it still remains to be checked whether TW2 and MS-A are the same. The mirror-symmetric solution of HPF found by our homotopy continuation corresponds to that of [14].

We believe that the mirror-symmetric disturbances play an important role in transition to turbulence in shear flows, in general.

Acknowledgments The author would like to acknowledge Professor D. P. Wall and Dr. K. Deguchi for their contributions towards the compilation of the author's study on the connection between exact coherent structures in shear flows. This article was completed while the author was staying at Tianjin University as recruited by the '1000 Talents Plan' in China.

Compliance with ethical standards

Conflict of interest The author declares that he has no conflict of interest.

Funding This study was funded by the National Science Foundation of China (Grant number:115722).

References

1. Romanov VA (1973) Stability of plane parallel Couette flow. Funct Anal Appl 7:137–146
2. Meseguer A, Trefethen LN (2003) Linearized pipe flow to Reynolds number 10^7. J Comput Phys 186:178–197
3. Reichardt H (1959) Über die Geschwindigkeitsverteilung in einer geradlinigen turbulenten Couetteströmung. Z Angew Math Mech 36:26–29
4. Reynolds O (1883) An experimental investigation of the circumstances which determine whether the motion of water shall be direct or sinuous and of the law of resistance in parallel channels. Philos Trans R Soc Lond 174:935–982
5. Nagata M (1990) Three-dimensional finite amplitude solutions in plane Couette flow: bifurcation from infinity. J Fluid Mech 217:519–527
6. Faisst H, Eckhardt B (2003) Traveling waves in pipe flow. Phys Rev Lett 91:224502
7. Wedin H, Kerswell RR (2004) Exact coherent structures in pipe flow: travelling wave solutions. J Fluid Mech 508:333–371
8. Gibson JF, Halcrow J, Cvitanovic P (2009) Equilibrium and travelling-wave solutions of plane Couette flow. J Fluid Mech 638:243–266
9. Itano T, Generalis SC (2009) Hairpin vortex solution in plane Couette flow: a tapestry of knotted vortices. Phys Rev Lett 102:114501
10. Deguchi K, Nagata M (2010) Traveling hairpin shaped fluid vortices in plane Couette flow. Phys Rev E 82:056325-1–056325-5
11. Waleffe F (2003) Homotopy of exact coherent structures in plane shear flows. Phys Fluids 15(6):1517–1534
12. Nagata M, Deguchi K (2013) Mirror-symmetric exact coherent states in plane Poiseuille flow. J Fluid Mech 735:R4-1–R4-11
13. Wall DP, Nagata M (2016) Exact coherent states in channel flow. J Fluid Mech 788:444–468
14. Pringle CCT, Kerswell RR (2007) Asymmetric, helical and mirror-symmetric traveling waves in pipe flow. Phys Rev Lett 99(2):074502
15. Nagata M, Busse FH (1983) Three-dimensional tertiary motions in a plane shear layer. J Fluid Mech 135:1–26
16. Wall DP, Nagata M (2013) Three-dimensional exact coherent states in rotating channel flow. J Fluid Mech 727:533–581
17. Nagata M (2013) A note on the mirror-symmetric coherent structure in plane Poiseuille flow. J Fluid Mech 727:R1-1–R1-8
18. Nagata M (1999) Ribbons in rotating plane Couette system, In: Egbers C, Pfister G (eds) Proceedings of 11th international couette-taylor workshop. Bremen, Germany, pp 67–68
19. Lezius DK, Johnstone JP (1976) The structure and stability of turbulent boundary layers in rotating channel flow. J Fluid Mech 77:153–175
20. Deguchi K, Nagata M (2011) Bifurcations and instabilities in sliding Couette flow. J Fluid Mech 678:156–178
21. Eisen H, Heinrichs W, Witsch K (1991) Spectral collocation methods and polar coordinate singularities. J Comput Phys 96:241–257
22. Deguchi K (2013) Ph. D. Thesis, Kyoto University
23. Deguchi K, Nagata M (2016) Connection between exact coherent states in plane Couette flow and pipe flow (in preparation)